Contaminant containment using polymer gel barriers

M.I.M. Darwish, R.K. Rowe, J.R.C. van der Maarel, L. Pel, H. Huinink, and P.L.J. Zitha

Abstract: Polymer gels are well known in the oil industry, but their potential for use as barriers to contaminant transport has not previously received significant study. As a first step, this paper examines the potential for a polyelectrolyte gel to serve as a barrier to the migration of sodium chloride. Two series of tests are reported. These involve the use of hydrogen pulsed field gradient – nuclear magnetic resonance (HPFG–NMR) to measure the self-diffusion on a microscopic scale and the use of magnetic resonance imaging (MRI) to monitor Na^+ and H^+ migration in the polymer gel with time. It is shown that the gel, which has a hydraulic conductivity of 2×10^{-12} m/s, has a diffusion coefficient similar to that of compacted clay and greater sorption of Na^+ than is typical for compacted clay.

Key words: diffusion, contaminant, osmosis, gels, barriers.

Résumé : Les gels de polymère sont bien connus dans l'industrie pétrolière, mais leur potentiel comme barrières au transport de contaminants n'a pas été jusqu'à ce jour l'objet d'études significatives. Dans une première étape, l'article examine le potentiel de gel polyélectrolyte pour servir de barrière à la migration du chlorure de sodium. On rapporte deux séries d'essais. Ceux-ci impliquent l'utilisation d'une source magnétique nucléaire avec gradient d'hydrogène pulsé sur le terrain (HPFG–NMR) pour mesurer l'autodiffusion à l'échelle microscopique, et l'utilisation d'image de source magnétique (MRI) pour mesurer la migration de Na^+ et H^+ dans le gel de polymère en fonction du temps. On montre que le gel, qui a une conductivité hydraulique de 2×10^{-12} m/s, a un coefficient similaire à celui de l'argile compactée et une plus grande sorption de Na^+ que celle typique pour l'argile compactée.

Mots clés : diffusion, contaminant, osmose, gels, barrières.

[Traduit par la Rédaction]

Introduction

The remediation of contaminated sites typically involves one or more of three basic strategies: containment, treatment, and (or) removal. The focus of this paper is on containment of inorganic contaminants using low-permeability barrier systems to control the migration of potential pollutants to negligible levels. Containment may be either the entire remediation strategy or part of a strategy that includes other techniques, such as pump and treat, soil flushing, alcohol, and flooding. In these cases the barrier helps reduce the risk of spreading mobilized contaminants beyond affected areas while the other techniques are implemented.

Containment barriers are selected for their ability to control pollutant flow and absorb suspended or dissolved pollutants (Haxo 1981). Currently, containment typically involves the use of cutoff curtains, slurry walls, geomembranes, geosynthetic clay liners, or compacted clay liners where each has advantages and disadvantages, with composite systems frequently being used to balance the advantages and disadvantages of the different components (Rowe 2001). Suspension grouts (e.g., cement, bentonite, and cement–bentonite grouts) have also been used in the construction of barriers. The injection of suspension grouts is restricted to coarse-grained sand deposits, however, and they are not suitable for sites requiring a deep penetration of the grout (Rumer and Ryan 1995).

Chemical grouts have the potential to provide containment without the need for excavation. They can be used in conjunction with a wide range of contaminants and have an advantage over other grouts in that they enable better control of the material properties such as viscosity and set time (Bodocsi and Bowers 1991). As a consequence, chemical grouts can be used in areas where the accessibility is insufficient for the installation of the other types of barriers (Rumer and Ryan 1995).

Polymers and gels have been widely used in the oil industry to enhance oil recovery (Zaitoun et al. 1991; Liang et al. 1993; Zitha and Darwish 1999). These materials also have

Received 17 October 2002. Accepted 22 August 2003. Published on the NRC Research Press Web site at http://cgj.nrc.ca on 4 February 2004.

M.I.M. Darwish and P.L.J. Zitha. Delft University of Technology, Faculty of Civil Engineering and Geosciences, Mijnbouwstraat 120, 2628 RX Delft, The Netherlands.
R.K. Rowe.[1] Department of Civil Engineering, Queen's University, Mackintosh–Corry Hall, Room F407, Kingston, ON K7L 3N6, Canada.
J.R.C. van der Maarel. Leiden University, P.O. Box 9502, 2300 RA Leiden, The Netherlands.
L. Pel and H. Huinink. Eindhoven University of Technology, Den Dolech 2, Box 513, 5600 MB Eindhoven, The Netherlands.

[1]Corresponding author (e-mail: kerry@civil.queensu.ca).

 doi: 10.1139/T03-072

the potential to be used as a barrier (e.g., as a grout or a slurry) for containment of contaminants, but they have received little attention in the literature. Polymer chains are macromolecules consisting of a high number of units (monomers) bonded together. These units may be charged or neutral. The charged polymers (polyelectrolytes) can be negatively or positively charged, with the degree of charge depending on the number of charged units. Water-soluble polymers dissolve in water and form a polymer solution that contains polymer chains. When the cross-linker (i.e., a specific chemical) is added, the individual chains are connected together at a number of points to form a three-dimensional polymer chain network analogous to a porous medium with the solvent (e.g., the water with which the gel was prepared) filling the pores between the polymer chains. For charged polymer solutions, the charges are neutralized by the presence of ions with opposite charge (i.e., counter-ions). The hydraulic conductivity of the gel is analogous to that of a porous medium and represents the resistance of the gel to water flow due to a hydraulic gradient. The hydraulic conductivity of the gel used in this study was 2×10^{-12} m/s.

The objective of this paper is to evaluate the ability of a novel polyelectrolyte gel to form a barrier to control the migration of inorganic contaminants. The gel appears to be an excellent candidate to form a viscous liquid barrier (VLB), which is a barrier formed by the injection of viscous liquids that gel, in situ, after a certain predesigned time (Apps et al. 1998). Alternatively, polyelectrolyte gels can be mixed with sand to form a lateral barrier or for use as a component of composite liner systems. It may be hypothesized that with appropriate design such a gel-based barrier would help reduce the diffusive flux to a rate within the dispersion and dilution capacity of the local groundwater. To design such a system, however, one would need to know the diffusion and sorption parameters of the contaminants of interest for the gel barrier. Thus, the objective of this paper is to study contaminant diffusion through a gel barrier. Two series of tests are reported. First, four sets of hydrogen pulsed field gradient – nuclear magnetic resonance (HPFG–NMR) experiments are used to measure the self-diffusion coefficients of ions on a microscopic scale to verify the model developed in this work. Second, magnetic resonance imaging (MRI) measurements are used to measure the Na^+ and H^+ migration in the gel with time, and the results are compared with the calculations based on the predicted diffusion coefficients using the model verified by the NMR experiments. Batch experiments were conducted to estimate the sorption parameters.

Background

Diffusion of ions in gel barriers

Field studies have shown that the most important contaminant transport mechanism for very low permeability barriers is molecular diffusion (Goodall and Quigley 1977; Crooks and Quigley 1984; Rowe et al. 1995). Thus it may be anticipated that diffusion would be a key consideration with respect to the use of polyelectrolyte gels as potential barriers to the migration of ions.

Membrane behavior, or the ability of the gel to impede the passage of solute through the gel, involves the restriction of the passage of charged solute (ions) through the pores of charged gel due to electrostatic repulsion of the ions by electric fields associated with diffuse double layers of adjacent network chains. This is analogous to what was observed for clay soils (Cey et al. 2001).

Microscopic diffusion

A model describing the microscopic diffusion of ions through polyelectrolyte gels has been described in detail by Darwish et al. (2001). The following summarizes the key aspects of the model.

An obstruction-scaling model for the diffusion of an uncharged solute in an uncharged homogeneous hydrogel, proposed by Amsden (1999), gives

$$[1] \qquad \frac{D_g}{D_0} = \exp\left[-\frac{\pi}{4}\left(\frac{r_s + r_f}{\bar{r} + r_f}\right)^2\right]$$

where D_g and D_0 are solute diffusion coefficients in gel and water (m^2/s), respectively; r_s is the hydrodynamic radius of the solute molecule (m); r_s is the polymer chain radius (m); $\bar{r}$ is the average radius of the openings between the polymer chains; and $r_s + r_f$ is the critical limiting radius required to permit solute passage (m).

From the Stokes–Einstein equation, knowing the diffusion coefficient of the solute in the solvent and assuming that the solute and the solvent molecules are of the same size, the hydrodynamic solute radius, r_s, can be calculated from

$$[2] \qquad r_s = k_B T / 4\pi\eta D_0$$

where k_B is the Boltzmann constant (J/° K), T is the absolute temperature (K), and η is the solvent viscosity at the temperature at which D_0 was obtained (Pa·s).

The average radius of the openings between the polymer chains can be defined by using scaling methods to characterize the gel (De Gennes 1979). Thus, the opening radius can be taken as equal to half the correlation length (i.e., $\bar{r} = \xi/2$, where ξ is the correlation length of the polymer in solution), and this can be substituted in eq. [1]. The polymer chain correlation length is defined as the distance beyond which the dynamic movement of different chain segments is not felt by another segment (i.e., not correlated).

This model only accounts for the geometrical obstruction due to the presence of the polymer network. For electrostatically interacting charged solutes and a charged polymer network (e.g., diffusion of ions in polyelectrolyte gels) one also needs to account for the electrostatic obstruction by introducing an effective ion radius for the ions moving into the charged polymer network. Thus, the critical limiting radius required to permit solute passage through the network is taken as the effective ion radius. The difference between the hydrodynamic and the effective ion radii was taken as the distance at which the electrostatic potential equals the thermal energy. This depends on the salt concentration and can be calculated by solving the Poisson–Boltzmann equation for the electrostatic potential around the polymer chain. The ratio between the effective self-diffusion coefficient for ions (cations or anions) in polyelectrolyte gels and that in water or the apparent tortuosity factor, $\tau_a(c_s)$, can be written as

$$[3] \qquad \tau_a(c_s) = \frac{D_g(c_s)}{D_0} = \exp\left[-\frac{\pi}{4}\left(\frac{r_s^e + r_f^e}{\xi_{ns}/2 + r_f^e}\right)^2\right]$$

where $\tau_a(c_s)$ is the apparent tortuosity factor at a salt concentration c_s (g/m^3), $D_g(c_s)$ is the effective diffusion coefficient in gel (m^2/s), r_s^e is the effective radius of ions (m), r_f^e is the polymer chain effective radius (m), and ξ_{ns} is the correlation length for the case with no salt (m). Using scaling laws (Dobrynin et al. 1995), the correlation length for the case with no salt added, ξ_{ns}, and the effective chain radius, r_f^e, in a semidilute polyelectrolyte solution can be calculated as indicated in Appendix A.

Macroscopic diffusion

The solute (ion) transport equation, taking adsorption and advection (due to osmotic flow) into account, is

$$[4] \qquad \frac{\partial[c_s + \psi(c_s)]}{\partial t} = \frac{\partial}{\partial x}\left[D_g(c_s)\frac{\partial c_s}{\partial x}\right] - \frac{\partial}{\partial x}[\nu(c_s)c_s]$$

where x is the distance, t is the time, $\sigma(c_s)$ is the ion (e.g., sodium) concentration in the pores of the gel (bearing in mind that the polymer chain network forms a porous media and the original water is the pore fluid) (g/m^3), $\psi(c_s)$ is the ion adsorption density on the polymer network (g/m^3), and $v(c_s)$ is the osmotic flux (g/(m^2·s^{-1})). The adsorption density is given by

$$[5] \qquad \psi(c_s) = (\rho/\theta)K_d(c_s)c_s$$

where ρ, θ, and $K_d(c_s)$ are, respectively, the density of the dry polymer (g/m^3), the volume fraction of the polymer in the gel, and the partitioning coefficient of the ion solute (mL/g). The osmotic flux velocity (m/s) (Barbour and Fredlund 1989) modified to reflect the concentration dependence is given by

$$[6] \qquad \nu(c_s) = \sigma(c_s)k_h\frac{d\Pi}{dx}(c_s)$$

where $\sigma(c_s)$ is the osmotic efficiency, k_h is the gel hydraulic conductivity (m/s), and $d\Pi/dx(c_s)$ is the osmotic pressure gradient. The osmotic efficiency, $\sigma(c_s)$, was calculated from Bresler (1973), and the osmotic pressure gradient, $d\Pi/dx(c_s)$, was calculated from Mitchell (1993) as follows:

$$[7] \qquad \Pi = RT\sum(c_{ic} - c_{io})$$

where Π is the osmotic pressure (kPa); R is the gas constant (0.0083145 m^3·kPa·mol^{-1}·K^{-1}); T the absolute temperature; and c_{ic} and c_{io} are, respectively, the midplane (i.e., in the middle between two adjacent chains) and equilibrium (i.e., in the bulk solution away from the chains) cation and anion concentrations (mol/m^3) deduced by solving the Poisson–Boltzmann equation. Concentrations c_{ic} and c_{io} are defined in greater detail by Bolt (1956).

Equation [4] was solved using the finite element based software FlexPDE™ (Backstrom 2002) for the initial and boundary conditions described later in the paper.

Experimental

Gel preparation

Partially hydrolyzed (i.e., negatively charged) polyacrylamide polymers with a 25% degree of hydrolysis and molecular weight of 100 000 g/mol at a concentration of 20% active material, by mass, were dissolved in water to form a polymer solution. Glyoxal with 40%, by mass, concentration in water was used as a cross-linker. The gel was prepared by mixing the three components (cross-linker solution, distilled water, and polymer solution) while stirring until a homogenous solution was obtained. Subsequently, these homogenous solutions were placed in an oven at 50 °C to let gelation take place. Different proportions of cross-linker were examined by mixing between 2.5% and 25%, by volume, cross-linker with 47.5%–25% distilled water, the balance of 50% being the polymer solution.

Batch experiments

The effect of salt content on the distribution coefficient $K_d(c_s)$ was examined using batch experiments. In these experiments, different gel samples were prepared in Teflon tubes of 20 mm height and 15 mm diameter with open ends covered with a tightly connected thin sheet of porous Teflon to prevent swelling. Each sample was then placed in a 500 mL NaCl solution for a range of NaCl concentrations between 8.5 and 170 mol/m^3. The samples were continuously agitated and left to equilibrate with the salt solution at 25 °C. After equilibrium, samples were removed from the solution, carefully wiped, and immersed in a known volume of double distilled water. Care was taken to ensure that the volume of distilled water was sufficient to free practically all the sorbed Na^+ and small enough to allow for Na^+ detection based on a knowledge of Na^+ solubility in water and the detection range of the ion selective electrode. The Na^+ concentration was monitored with time using an ion-selective electrode until the concentration reached a constant value C_{sf} (g/m^3). The amount of absorbed mass of Na^+ per unit mass of the gel, q, was calculated from

$$[8] \qquad q = \frac{M_{Na}}{M_g} = \frac{C_{sf}V_w}{(1-\theta)V_g\rho_g}$$

where M_{Na} is the mass of adsorbed Na^+ (g), M_g is the mass of the polymer network (g), V_w is the water volume used to desorb the sodium (mL), θ is the gel porosity, V_g is the gel volume (mL), and ρ_g is the polymer network dry density (g/m^3). Subsequently, an adsorption isotherm was developed and the partitioning coefficient $K_d(c_s)$ was calculated.

NMR spectroscopy

Four sets of hydrogen pulsed field gradient – nuclear magnetic resonance (HPFG–NMR) experiments were conducted to measure the self-diffusion coefficients of the ions of interest in both water and gel. The objective of these series of experiments was to verify the model for diffusion developed in this work. The gel samples were prepared using heavy water (D_2O) to avoid the overlap between the ion and water signals. The gel samples were then put into special NMR glass tubes with 4 mm inner diameter, before gelling, to a height of 4 mm and the tubes were put in the oven at

50 °C until gelation took place. The salt solutions, at different salt concentration (between 8.5 and 170 mol/m^3), were then put on top of the gel samples to a height of 4 mm. The gel samples and salt solutions were left until equilibrium was reached, as indicated by measuring the salt self-diffusion in the sample using NMR with time until a constant value was recorded.

Three different salt solutions were used: tetra-methyl-ammonium chloride TMA^+Cl^- ($(CH_3)_4{\cdot}NCl$) was used as an organic monovalent salt, putrescine Pu ($H_2N{\cdot}(CH_2)_4{\cdot}NH_4$) was used as an organic divalent salt, and sodium butyrate ($CH_3CH_2CH_2CO_2Na$) was used as an organic monovalent salt.

The first set of experiments provided baseline results by examining the water diffusion coefficient for several cross-linker contents in the gel without added salt. The second set of experiments was aimed at measuring the diffusion coefficient of the monovalent organic cations for several salt concentrations. The third set of experiments was performed to obtain the diffusion coefficient of the divalent organic cations at different salt concentrations. The fourth set of experiments was carried out to establish the diffusion coefficients of monovalent organic anions for several salt concentrations.

Magnetic resonance imaging (MRI)

The primary purpose of the MRI measurements was to verify the model developed in this study, for ion diffusion, on a macroscopic scale. Gel samples were placed to a height of about 6 cm in 10 cm high Perspex™ cylinders (2.5 cm inner diameter), and the remaining 4 cm was filled with NaCl solution at an initial concentration, c_o, of 170 mol/m^3. The gel was prevented from swelling, to simulate the gel in the porous medium, by fitting a thin sheet of porous Perspex™ on top of the sample. The MRI was used to measure the sodium and hydrogen ion concentration profiles in both the NaCl solution and the gel body, at certain elapsed times, while the samples were held vertically and the salt solution was on top. The Na^+ and H^+ concentrations were averaged over every 6 mm in the salt solution side and every 1 mm at the solution–gel interface region, increasing to 2 mm and then to 4 mm in the gel body. The experiments described in this paper were conducted using an NMR scanner that incorporates an iron-cored electromagnet operating at a field of 0.78 T (Pel et al. 2000).

Results and discussion

Gelling time

For given applications, the gelling time of the barrier liquids must fit within a time window that is long enough to allow comfortable emplacement and prevention of premature gelling but sufficiently short to prevent excessive drainage and redistribution in the soil.

To assess the gelling time, the gel rheological properties were investigated using an advanced rheometric expansion system (ARES) with couette system (cup diameter 33.9 mm, bob diameter 32 mm, height 33.3 mm), at different temperatures, pH values, and percentages of cross-linker.

Figure 1 shows the elastic (storage modulus G') and viscous (loss modulus G'') components of viscoelasticity and the viscosity η with time for 7.5% added cross-linker at 50 °C. The loss modulus, G'', represents the energy dissipated (e.g., as heat), and the storage modulus, G', represents the energy stored in the microstructural links in the solid body when external work is applied to the viscoelastic body (i.e., gel). The loss modulus and the storage modulus represent the liquid-like and solid-like behaviors of the gel, respectively.

The gelling time is taken, as conventionally, to be the time at which there is a crossover of G' and G'' when the measurements are done using a constant frequency. Based on rheological studies (Tung and Dynes 1982), this point in time was chosen to represent the gelling time because it is the point at which a gel network in the total bulk volume starts to appear. This gelling time (i.e., time when $G' = G''$) agrees well with the gel time determined by the American Society for Testing and Materials (ASTM) standard method. The development of the gel network structure as reflected by the increase in the storage modulus G' and loss modulus G'' is shown in Fig. 2. Initially the system behaved like a liquid (i.e., the storage modulus was strongly dependent on the frequency and $G'' > G'$); however, as the network developed, the low-frequency storage modulus became nearly independent of frequency (i.e., the system then had a rubber-like behavior). The almost horizontal part of the curves is called rubber plateau, and the value of G' in this interval is called the equilibrium shear modulus G_e. The gelling time (Ming et al. 1997) can be adjusted to be suitable for different site conditions by altering either the temperature or the pH as shown in Table 1 for gel alone. These values could change when sand is present.

Although jar tests (Sydansk and Argabright 1987) are a fast and easy way to estimate the gelling time in the presence of sand, they cannot provide the quantitative data needed for reliable prediction, including numerical simulation, of grout injection and gelling behavior. Such quantitative data can be obtained from rheological measurements similar to those used here.

Batch experiments

The convex nonlinear Freundlich adsorption isotherm for sodium in the anionic gel is shown in Fig. 3. Since the adsorption isotherm is nonlinear, secant lines were used to estimate the partitioning coefficient and are also shown in Fig. 3. The secant lines were based on the following formulation for the partitioning coefficient $K_d(c_s)$ (Davidson et al. 1976):

$$[9] \qquad K_d(c_s) = \left.\frac{\Delta q}{\Delta c}\right|_{c_s} = \frac{q|_{c_s} - q|_{c=0}}{c_s - 0} = \frac{K_f c_s^N}{c_s} = K_f c_s^{N-1}$$

where q is the mass of solute sorbed per mass of gel, c_s is the initial concentration of Na^+ before exposure of the salt solution to the gel (g/m^3), and K_f and N are Freundlich isotherm parameters given by

$$[10] \qquad q = K_f c^N$$

with $K_f = 5.918 \times 10^{-9}$ and $N = 1.5967$. The values for Freundlich isotherm parameters were found by fitting the measured values of q, in Fig. 3, with eq. [10].

Fig. 1. Changes in storage modulus G', loss modulus G'', and complex viscosity with time for a mixture of 7.5% cross-linker, 42.5% distilled water, and 50% partially hydrolyzed polymer solution at 50 °C and 10 rad/s frequency.

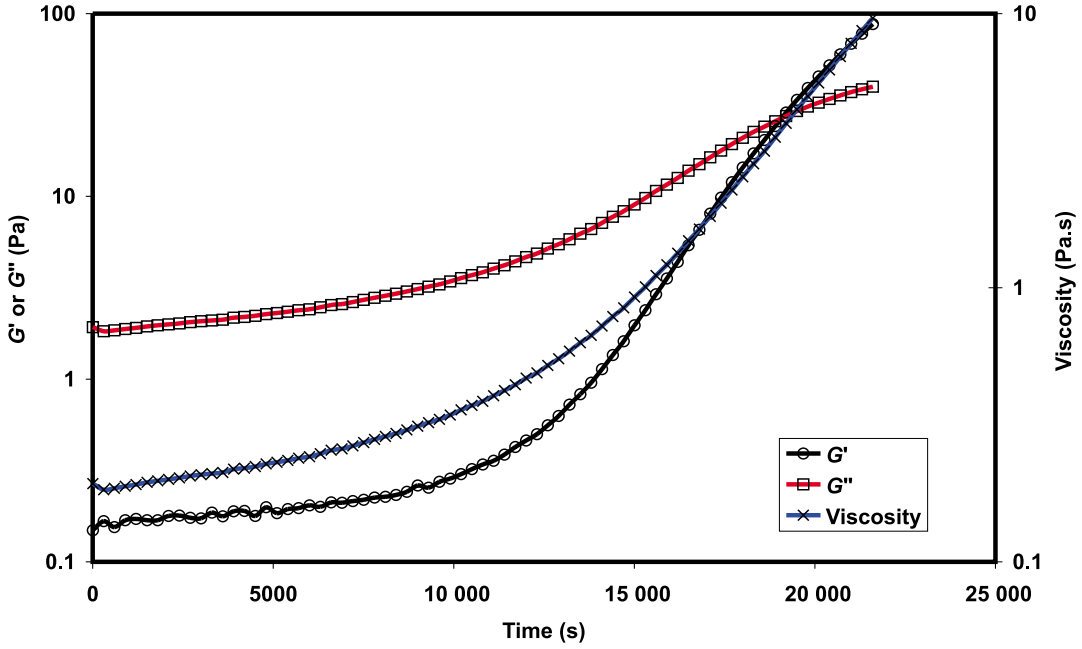

Fig. 2. Changes in storage modulus G', loss modulus G'', and complex viscosity for a mixture of 7.5% cross-linker, 42.5% distilled water, and 50% partially hydrolyzed polymer solution with frequency in the range from 0.1 to 100 rad/s at 50 °C.

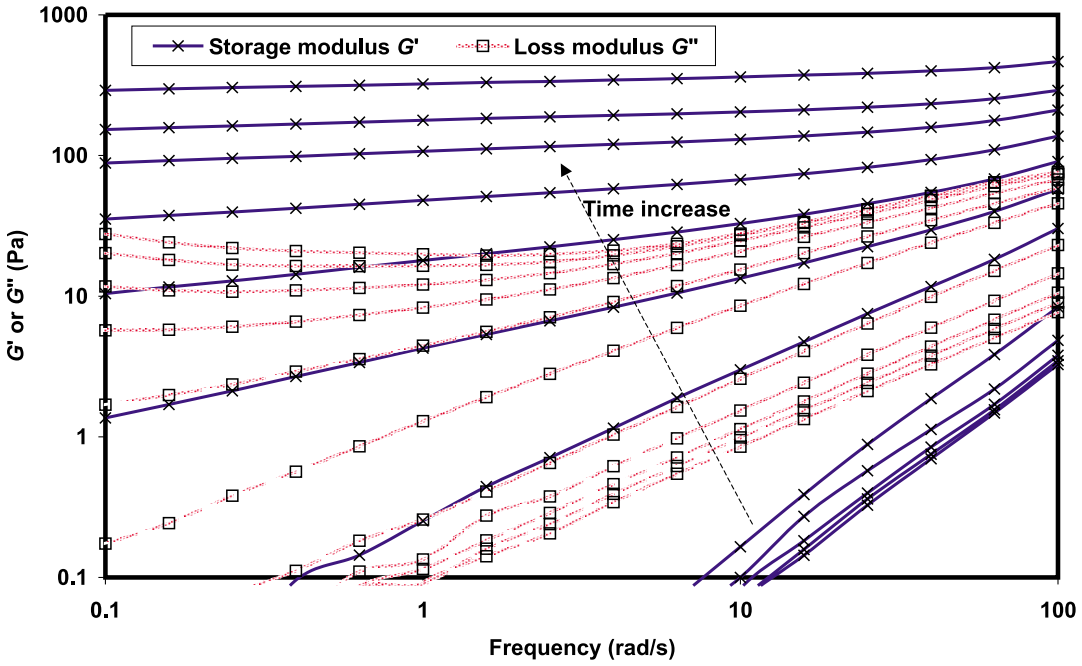

The amount of absorbed Na^+ ions increases with an increase in the initial Na^+ content. At a low initial Na^+ concentration, however, the Na^+ absorption rate is less than that at a higher Na^+ concentration. The $K_d(c_s)$ values, at a high initial Na^+ concentration, are higher than typical values for clay.

Diffusion coefficients

A series of experiments were performed to find the optimum amount of cross-linker material needed to satisfy the available cross-link sites in the polymer network without affecting its average opening. The data, in terms of a plot of the diffusion coefficients of water in the gel (D_w) versus the cross-linker content (volume percent), are given in Fig. 4. The data show that (*i*) for very low amounts of added cross-linker, there is hardly any effect on the water diffusion coefficient; (*ii*) for high amounts of added cross-linker, the water diffusion coefficient changes linearly with the logarithm of the cross-linker concentration; and (*iii*) for moderate amounts of cross-linker, there is a transition zone. The crossover between the two regimes occurred at 7.5% of added cross-

Fig. 3. Adsorption isotherm and the partitioning coefficient $K_d(c_s)$ calculated from eqs. [9] and [10] for sodium in an anionic gel at 25 °C.

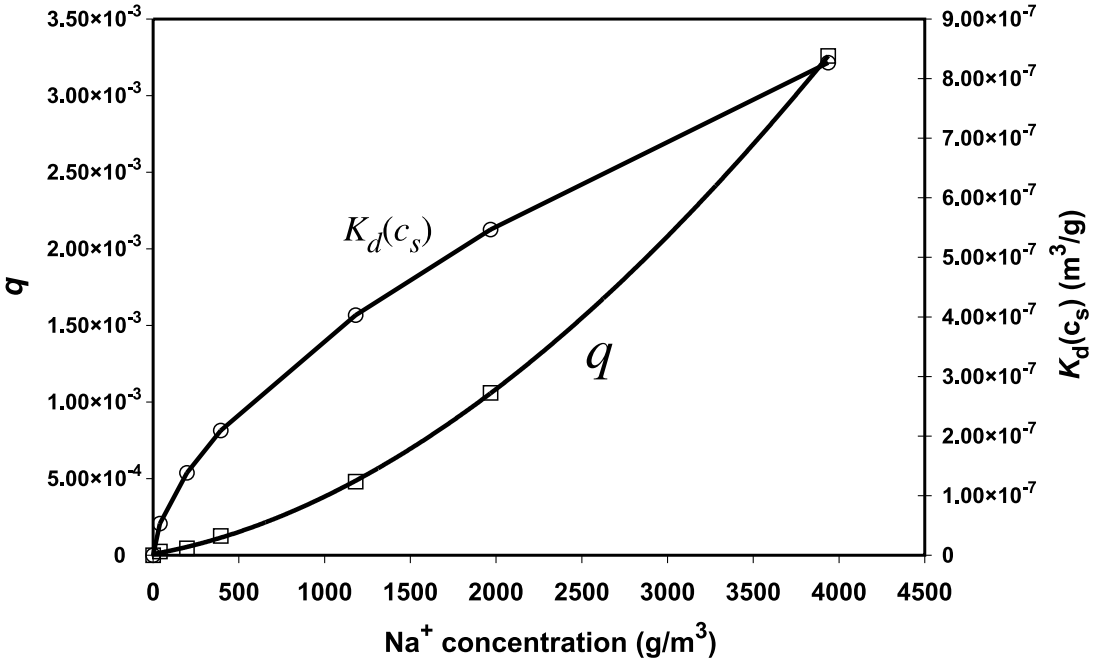

Fig. 4. Diffusion coefficients for water (D_w) in the gel versus gel cross-linker content.

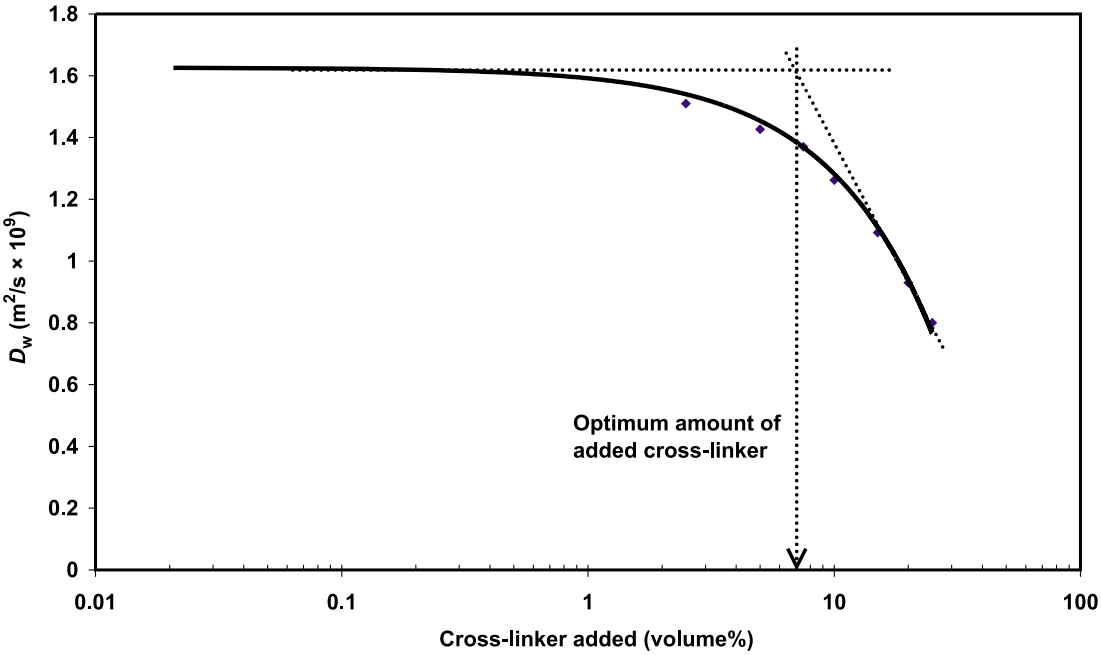

Table 1. Gelling times for different gel samples with different pH values, temperatures, and percent cross-linker added.

Sample No.	pH	Temp. (°C)	Cross-linker (vol.%)	Gelling time (h)
1	5.85	50	2.5	6.27
2	5.85	50	5.0	5.88
3	5.85	50	7.5	5.33
4	5.85	60	7.5	3.73
5	7.00	50	7.5	1.13
6	8.00	30	7.5	0.10

linker, which was taken as the optimum amount of cross-linker to be added to satisfy the available cross-linking sites. In support of this optimum value, it is noted that the previous NMR measurements yielded a peak on the spectrum for cross-linker contents higher than 7.5%, and this was found to be due to the free cross-linker. In practice, the amount of added cross-linker could be designed to minimize the network opening and consequently the diffusion fluxes. In this study, however, care was taken to avoid affecting the average network opening so as to verify the model developed (i.e., eq. [3]).

Figure 5 shows the measured and predicted (using eq. [3])

Fig. 5. Measured and predicted apparent tortuosity factors for the organic monovalent cations (TMA) and water in the gel versus TMA concentration. The data points are means of 3 replicates, and the vertical bars represent standard deviation. X-linker, cross-linker.

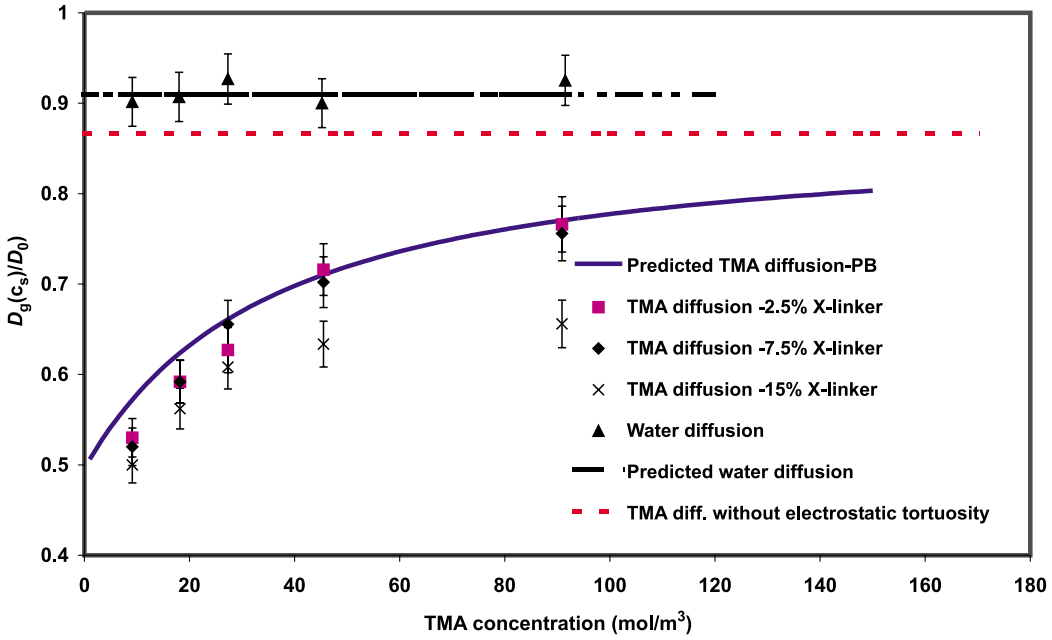

Fig. 6. Measured and predicted apparent tortuosity factors for the organic divalent cations (Pu) and water in the gel versus Pu concentration. The data points are means of 3 replicates, and the vertical bars represent standard deviation.

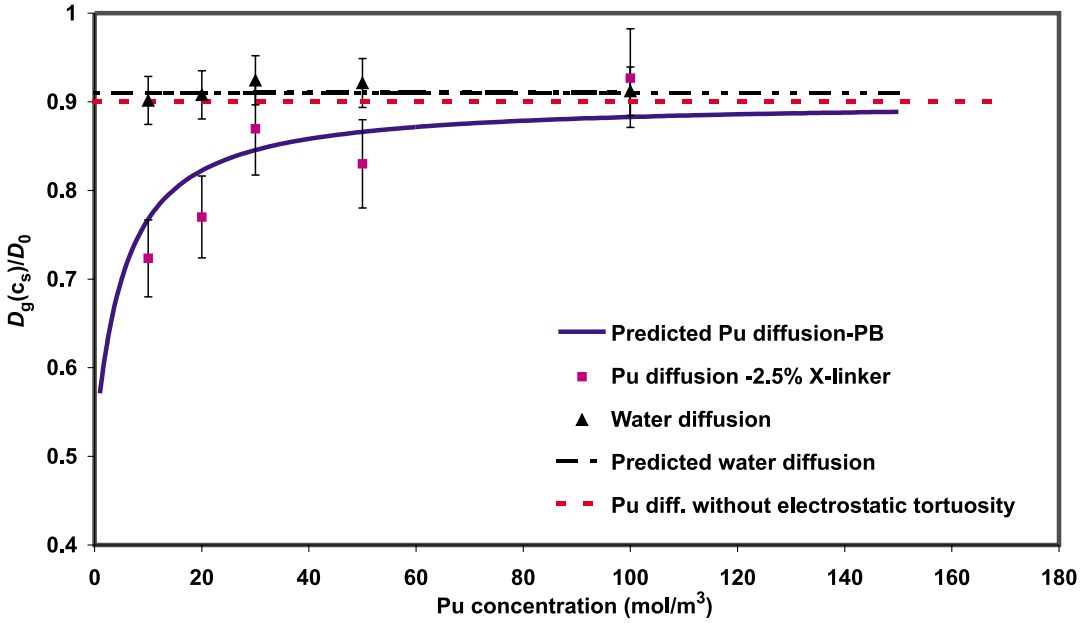

apparent tortuosity factors for the organic monovalent cations (TMA) in the gel as a function of TMA concentration. The apparent tortuosity factors were measured at different cross-linker contents (2.5%, 7.5%, and 15%). The predicted values, obtained using the solution of the Poisson–Boltzmann equation to predict the effective radius of the moving solute, agree well with the measured values up to 7.5% added cross-linker (Fig. 5). This is consistent with previous findings (Amsden 2001 for polyelectrolytes; and Lake and Rowe 2000 and Malusis and Shackleford 2002 for clay) and was attributed to the double-layer contraction. For 15% added cross-linker, the measured values deviated from the other results. This can be explained by the presence of free cross-linker that affects the average network opening and confirms the choice of the optimum amount of cross-linker based on the experiments discussed earlier. Figure 5 also shows the measured and predicted apparent tortuosity factors for water in the gel at different TMA concentrations for the gel containing 7.5% cross-linker (by volume). The predicted TMA apparent tortuosity factor without electrostatic interaction is also shown in Fig. 5.

The measured and predicted apparent tortuosity factors for

Fig. 7. Measured and predicted apparent tortuosity factors for the organic monovalent anions (butyrate) and water in the gel versus butyrate concentration. The data points are means of 3 replicates, and the vertical bars represent standard deviation.

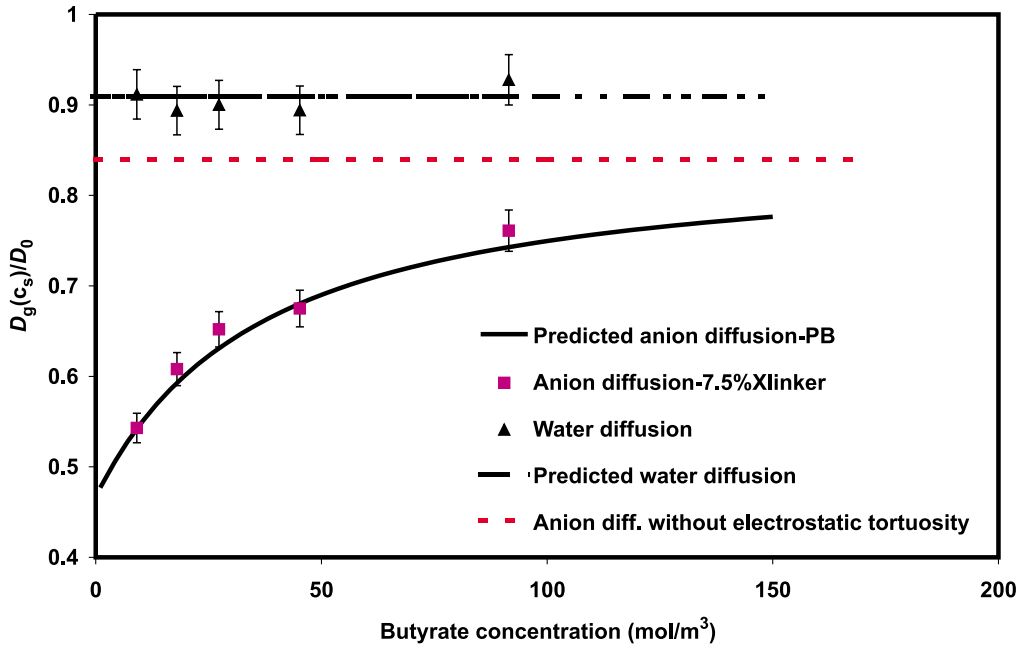

Fig. 8. Initial and final (i.e., after 8 days) normalized hydrogen concentration profiles through the source solution and gel. The data points are means of 3 replicates, and the vertical bars represent standard deviation.

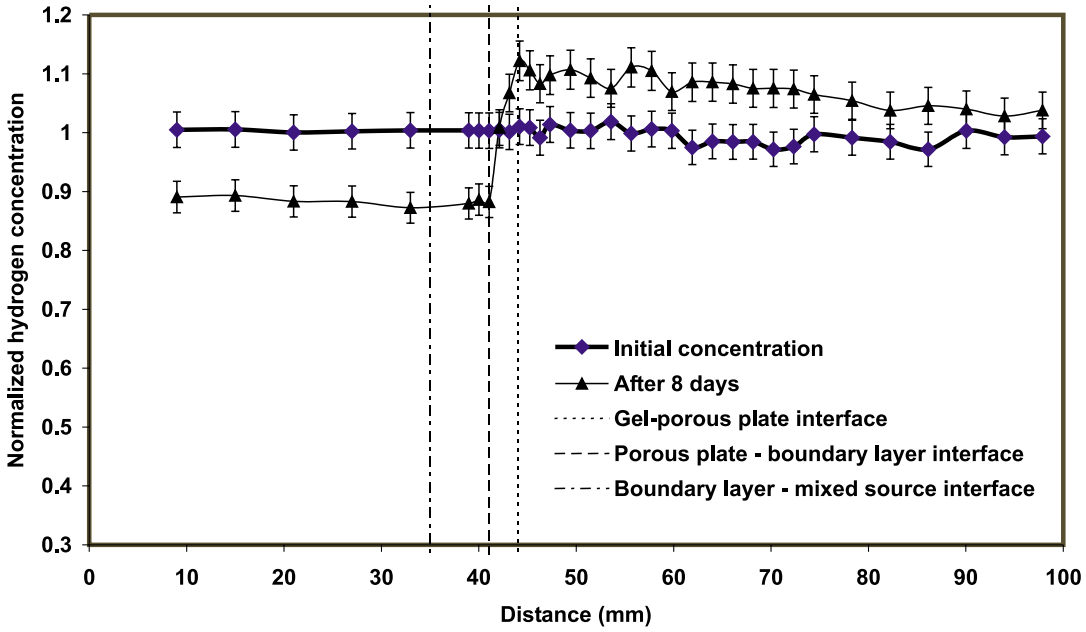

the organic divalent cation (Pu) in the gel at different Pu concentrations are shown in Fig. 6. There was reasonable agreement between the measured and predicted values, which also supports the validity of the model (i.e., eq. [3]) for divalent salts. Figure 6 shows the measured and predicted diffusion coefficient values for water in the gel at different Pu concentrations for the gel with 7.5% cross-linker by volume. In addition, Fig. 6 shows the predicted Pu apparent tortuosity factors without electrostatic interaction in the gel.

The apparent tortuosity factors for the organic monovalent anions (butyrate) in the gel at different butyrate concentrations are shown in Fig. 7. The experimental values are in excellent agreement with the theoretical prediction obtained using eq. [3] and based on Poisson–Boltzmann calculations to deduce the effective diameter of the moving solute. Figure 7 also shows the measured and predicted apparent tortuosity factors for water in the gel at different butyrate concentrations (for the gel containing 7.5% cross-linker by volume). These results show the validity of the model for diffusion of both cations and anions in the gel and

Fig. 9. Measured and calculated sodium ion concentration profiles in both the source solution and gel after 24, 48, 120, 168, and 192 h. The data points are means of 3 replicates, and the vertical bars represent standard deviation.

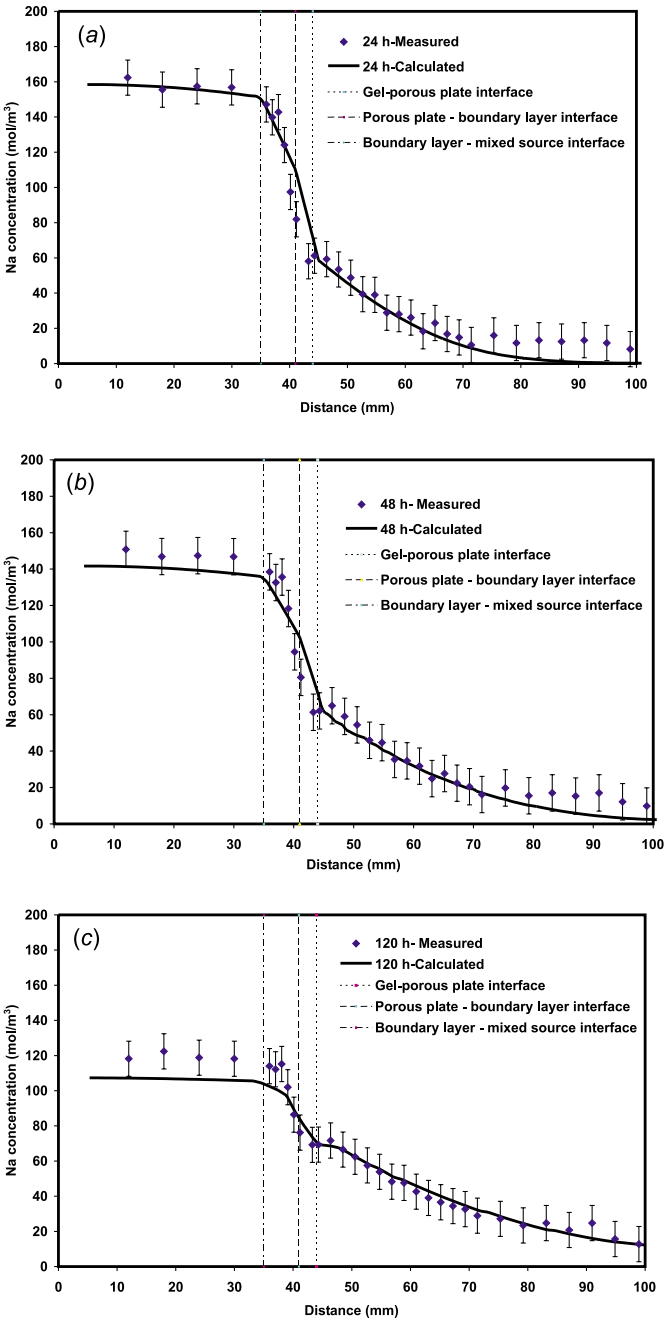

demonstrate that the expansion and contraction of the double layer is an important factor affecting ion diffusion (Rowe et al. 1995).

Macroscopic diffusion of H^+ and Na^+

The driving force for the migration of Na^+, Cl^-, NH^{4+}, and monomers (indicated by total organic carbon or TOC) is the chemical potential gradient, but for water the driving force is the osmotic pressure. To assess the relative importance of the migration of different species on the Na^+ migration, the

Fig. 9 (*concluded*).

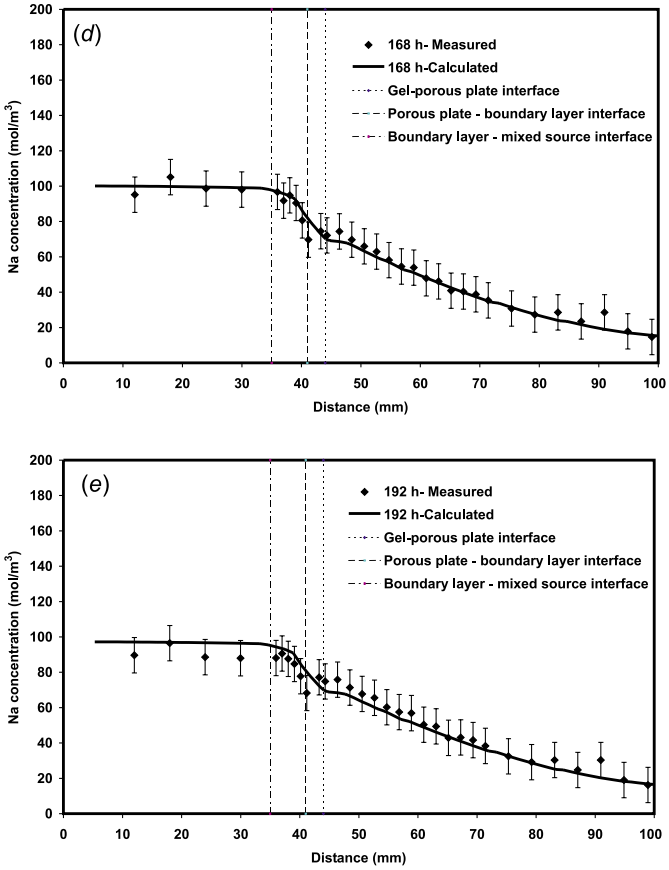

Fig. 10. Schematic showing the initial and boundary conditions for the MRI experiments. $c_s = c_o$ at $0 \le x \le b$ ($t = 0$); $c_s = 0$ at $b \le x \le L$ ($t = 0$); and $\partial c_s/\partial x = 0$ at $x = 0$ and $x = L$ ($t > 0$).

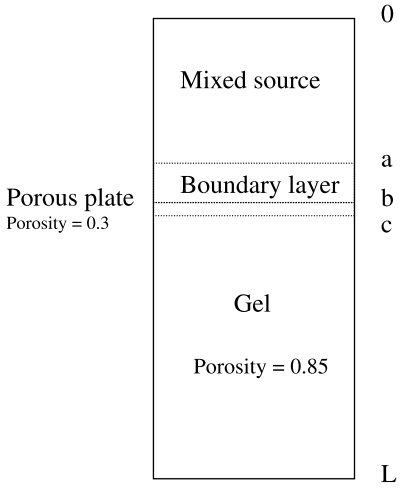

hydrogen and sodium concentration profiles were measured simultaneously at different times. Figure 8 shows the normalized hydrogen concentration profiles in both the source (salt solution) and gel with respect to the initial average concentration in the source and gel, respectively.

The hydrogen concentration profiles in Fig. 8 show a decrease in hydrogen concentration in the solution and a slight

Table 2. Values of the diffusion and partitioning coefficients used in the calculations for each layer.

	Gel layer	Porous Perspex™ plate	Boundary layer	Source solution
Diffusion coefficient	Eq. [3]	Eq. [3] × plate porosity	13×10^{-10} m^2/s	10×10^{-9} m^2/s
Partitioning coefficient	Eq. [9]	Eq. [9]	0	0

Fig. 11. Osmotic flux from the salt solution into the gel. V is the velocity.

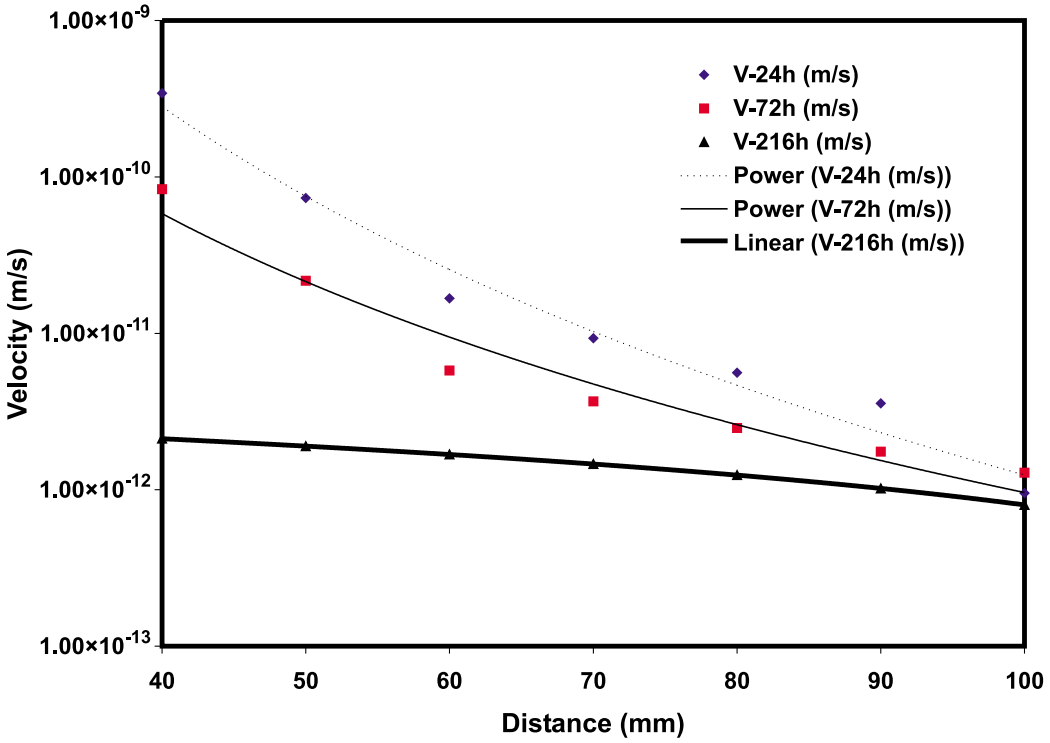

increase in the gel. These changes correspond to water movement under the effect of the osmotic pressure. The fact that there is water flux into the gel implies that the thin sheet of porous Perspex™ on top of the sample shifted slightly under the effect of the gel swelling pressure, allowing some volume change in the gel and hence providing an opportunity for some water to move into the gel. The change in hydrogen concentration also includes the effects of NH^{4+} and monomer migration out of the gel; however, the net mass transfer is towards the gel, which implies that water movement is the dominant process in terms of mass transport of hydrogen. The NH^{4+} and TOC concentrations were measured in the source solution and were consistent with this hypothesis.

Typical examples of the measured and calculated (using eq. [4]) sodium ion concentration profiles in both the solution and gel after 24, 48, 120, 168, and 192 h are shown in Fig. 9. The concentration profiles show the sodium concentration in the pores of the polymer network (i.e., the mobile sodium concentrations), Perspex™ plate, and source solution. The modeling of mass movement in the system involved consideration of four zones: the gel, the porous plate (with gel in pores), a boundary layer adjacent to the porous plate, and the main source solution. Each of these zones was modeled as a layer, with the source solution zone being "mixed" by the shaking that occurred during the scanning process. The calculated concentration profiles were obtained by solving eq. [4] with the initial and boundary conditions shown in Fig. 10. The values of the diffusion and partitioning coefficients that were used in the calculations, for each layer, are given in Table 2.

To calculate the osmotic flux from eq. [6] it was necessary to calculate the osmotic efficiency, $\sigma(c_s)$, and the osmotic pressure gradient, $d\Pi/dx(c_s)$. In these calculations, it was assumed that Na^+ and Cl^- were moving together and that the counter-ion distribution was uniform inside the gel. Thus, based on this assumption, the Cl^- concentration profile was predicted from the Na^+ concentration profile. The osmotic efficiency, $\sigma(c_s)$, was calculated knowing the mean Na^+ and Cl^- concentrations in the gel at each time step from the MRI measurements of the Na^+ concentrations. Knowing the mean Na^+ and Cl^- concentrations, the electrostatic potentials and the anion and cation distributions were obtained based on Kemper and Quirk (1970). Using these distributions, $\sigma(c_s)$ was calculated at each time interval based on Bresler (1973). As a check, the $\sigma(c_s)$ values obtained from this approach were comparable with those calculated by Cey et al. (2001).

Knowing the Na^+ and Cl^- concentration profiles in the gel at each time interval, the corresponding midplane concentration profiles were calculated, and the osmotic pressure was calculated from eq. [7], and thus $d\Pi/dx(c_s)$ was obtained and the osmotic flux calculated (eq. [6]) as shown in Fig. 11.

The osmotic flux starts at a relatively high values and then decreases with time until it reaches very small values as the system tends to equilibrium.

Although the diffusion and partitioning coefficients are concentration dependent, the average values were 5×10^{-10} m^2/s and 0.39 mL/g, respectively. Thus the average diffusion coefficient is comparable with that of clays (e.g., 4.8×10^{-10} m^2/s; Rowe et al. 1988), but the partitioning coefficient for the gel is higher than that typical for clays (e.g., 0.11 mL/g; Rowe et al. 1988).

From the results shown previously, the effective diffusion coefficients of ions passing through polymer gels are comparable with that for natural clays, but their absorptivity is higher than that of natural clays. The diffusivity may be decreased and the absorptivity increased by increasing the polymer or the cross-linker concentration because of the consequent decrease in the average network opening size and the increase in the available ion exchange sites, respectively. Increasing the cross-linker content will result in decreasing the gelling time as shown in Table 1 and increasing the value at which G' and G'' cross over each other.

Conclusions

Based on the findings from this series of tests, the following conclusions are drawn:

(1) The predictions using the obstruction model for the effective diffusion of ions (cations and anions of different valences) in polyelectrolyte gels, which takes into account the geometric and electrostatic obstructions, agreed well with the measurements for a broad range of salt concentrations.
(2) The measured average values for the gel barrier diffusion and partitioning coefficients suggest that the gel diffusion coefficient is comparable with that of natural clays, but the partitioning coefficient for the gel is higher than that typically encountered for clays.

These findings provide a preliminary indication that gels may have potential for use as a barrier, especially in situations where alternate systems are difficult to construct (e.g., in fractured media). More research is required to confirm the viability of this approach.

Acknowledgments

The discussion with Prof. S.L. Barbour and Mr. Bradley D. Cey with respect to modeling osmotic movement is gratefully acknowledged. The authors would like to express their gratitude to Jacques Kieffer and P. Thouilleux (SNF-Floerger™) for custom synthesizing the polymer samples used to carry out the experiment. The Dutch scientific research organization (NWO) is acknowledged for partially funding this work.

References

Amsden, B. 1999. An obstruction-scaling model for diffusion in homogeneous hydrogels. Macromolecules, **32**: 874–879.

Amsden, B. 2001. Diffusion in polyelectrolyte hydrogels: application of an obstruction-scaling model to solute diffusion in calcium alginate. Macromolecules, **34**: 1430–1435.

Apps, J.A., Persoff, P., Moridis, G., and Pruess, K. 1998. Method for formation of subsurface barriers using viscous colloids. U.S. Patent 5 836 390.

Backstrom, G. 2002. Fields of physics by finite element analysis: application to electricity, magnetism, and heat using FlexPDE version 3. GB Publishing, Malmo, Sweden.

Barbour, S.L., and Fredlund, D.G. 1989. Mechanisms of osmotic flow and volume change in clay soils. Canadian Geotechnical Journal, **26**: 551–562.

Bodocsi, A., and Bowers, M.T. 1991. Permeability of acrylate, urethane, and silicate grouted sands with chemicals. Journal of Geotechnical Engineering, ASCE, **117**(8): 1227–1244.

Bolt, G.H. 1956. Physico-chemical analysis of the compressibility of pure clay. Géotechnique, **6**(2): 86–93.

Bresler, E. 1973. Anion exclusion and coupling effects in nonsteady transport through unsaturated soils: I. Theory. Soil Science Society of America Proceedings, **37**: 663–669.

Cey, B.D., Barbour, S.L., and Hendry, M.J. 2001. Osmotic flow through a Cretaceous clay in southern Saskatchewan, Canada. Canadian Geotechnical Journal, **38**: 1025–1033.

Crooks, V.E., and Quigley, R.M. 1984. Saline leachate migration through clay: a comparative laboratory and field investigation. Canadian Geotechnical Journal, **21**: 349–361.

Darwish, M.I.M, Zitha, P.L.J, van der Maarel, J.R.C., Pel, L., and Huinink, H. 2001. Polymer gel barriers for waste disposal facilities. *In* Proceedings of the 14th Southeast Asian Geotechnical Conference, Hong Kong, 10–14 Dec. 2001. *Edited by* K.K.S. Ho and K.S. Li. A.A. Balkema, Rotterdam, The Netherlands. pp. 225–230.

Davidson, J.M., Ou, L.-T., and Rao, P.S.C. 1976. Behavior of high pesticide concentrations in soil water systems. EPA-600/9-76-015, U.S. Environmental Protection Agency, Cincinnati, Ohio. pp. 206–212.

De Gennes, P.-G. 1979. Scaling concepts in polymer physics. Cornell University Press, Ithaca, N.Y.

Dobrynin, A.V., Colby, R.H., and Rubinstein, M. 1995. Scaling theory of polyelectrolyte solutions. Macromolecules, **28**: 1859–1871.

Goodall, D.E., and Quigley, R.M. 1977. Pollutant migration from two sanitary landfill sites near Sarnia, Ontario. Canadian Geotechnical Journal, **14**: 223–236.

Haxo, H.E. 1981. Durability of liner materials for hazardous waste disposal facilities. *In* Proceedings of the 7th Annual Research Symposium, Land Disposal: Municipal Solid Waste. EPA-600/9-81-002a, U.S. Environmental Protection Agency, Cincinnati, Ohio, pp. 140–156.

Kemper, W.D., and Quirk, J.P. 1970. Graphic presentation of a mathematical solution for interacting diffuse layers. Soil Science Society of America Proceedings, **34**: 347–351.

Lake, C.B., and Rowe, R.K. 2000. Diffusion of sodium and chloride through geosynthetic clay liners. Geotextiles and Geomembranes, **18**: 103–131.

Liang, J., Lee, R.L., and Seright, R.S. 1993. Gel placement in production wells. SPE Production and Facilities (Nov. 1993), Transactions of AIME, **295**: 276–284.

Malusis, M.A., and Shackelford, C.D. 2002. Coupling effects during steady-state solute diffusion through a semipermeable clay membrane. Environmental Science and Technology, **36**: 1312–1319.

Ming, H., Muller, G., and Zaitoun, A. 1997. Gel formation of polyacrylamide in the presence of glyoxal for water control application. Polymer Gels and Networks, **5**: 471–480.

Mitchell, J.K. 1993. Fundamentals of soil behavior. John Wiley and Sons, New York.

Pel, L., Kopinga, K., and Kaasschieter, E.F. 2000. Saline absorption in calcium-silicate brick observed by NMR scanning. Journal of Physics D: Applied Physics, **33**: 1380–1385.

Rowe, R.K. 2001. Liner systems. *In* Geotechnical and geoenvironmental engineering handbook. *Edited by* R.K. Rowe. Kluwer Academic Publishing, Norwell, Mass. Chapt. 25, pp. 739–788.

Rowe, R.K., Caers, C.J., and Barone, F. 1988. Laboratory determination of diffusion and distribution coefficients of contaminants using undisturbed clayey soil. Canadian Geotechnical Journal, **25**: 108–118.

Rowe, R.K., Quigley, R.M., and Booker, J.R. 1995. Clayey barriers systems for waste disposal facilities. E&FN Spon, London, U.K.

Rumer, R.R., and Ryan, M.E. 1995. Barrier containment technologies for environmental remediation applications. John Wiley and Sons, New York.

Sydansk, R.D., and Argabright, P.A. 1987. Conformance improvement in a subterranean hydrocarbon-bearing formation using polymer gel. U.S. Patent 4 683 949.

Tung, C.Y.M., and Dynes, P.J. 1982. Relationship between viscoelastic properties and gelation in thermosetting systems. Journal of Applied Polymer Science, **27**(2): 569–577.

Zaitoun, A., Kohler, N., and Guerrini, Y. 1991. Improved polyacrylamide treatments for water control in producing wells. Journal of Petroleum Technology (JPT): 862–867.

Zitha, P.L.J., and Darwish, M.I.M. 1999. Effect of bridging adsorption on the placement of gels for water control. *In* Proceedings of the 1999 SPE Asia Pacific Improved Oil Recovery Conference, Kuala Lumpur, Malaysia, 25–26 Oct. 1999. CD-ROM. Society of Petroleum Engineers, Richardson, Tex.

Appendix A

Based on scaling methods (Dobrynin et al. 1995) developed to characterize gels, the correlation length, ξ_{ns}, for the case with no salt added satisfies

$$[A1] \quad \xi_{ns} \approx (B/cb)^{1/2}$$

where c is the polymer concentration, b is the monomer length, and $B \approx (A^2/u)^{2/7}$, in which A is the number of monomers between effective charges and $u = l_B/b$, where l_B is the Bjerrum length.

Thus, the effective chain radius r_f^e is scaled as follows, assuming that it is equal to the electrostatic blob radius:

$$[A2] \quad r_f^e \approx b(A^2/u)^{3/7}/2$$

Thus substitution of eqs. [A1] and [A2] into eq. [A3] gives

$$[A3] \quad D_r(c_s) = \exp\left\{-\frac{\pi}{4}\left[\frac{r_s + \delta(c_s) + k_s' b(A^2/u)^{3/7}/2}{k_s(B/cb)^{1/2} + k_s' b(A^2/u)^{3/7}/2}\right]\right\}$$

where $\delta(c_s)$ is the salt concentration dependent difference between the effective and hydrodynamic radius of the ions; and k_s and k_s' are the scaling constants, specific to a given polymer–water combination.

The scaling constants k_s and k_s' for the calculation of the correlation length ξ_{ns} and the effective chain radius r_f^e were obtained by fitting the three NMR sets of measurements to eq. [A3].